ACS APPLIED MATERIALS & INTERFACES

Research Article

www.acsami.org

High-Performance Inverted Solar Cells Based on Blend Films of ZnO Naoparticles and TiO_2 Nanorods as a Cathode Buffer Layer

Pandeng Li,[†,‡] Chunming Sun,[†] Tonggang Jiu,*[,†] Guojie Wang,[†] Jun Li,[†] Xiaofang Li,*[,‡] and Junfeng Fang*[,†]

[†]Institute of New Energy Technology, Ningbo Institute of Material Technology and Engineering (NIMTE), Chinese Academy of Science, Ningbo, Zhejiang 315201, People's Republic of China

[‡]School of Chemistry and Chemical Engineering, Hunan University of Science and Technology, Xiangtan, Hunan 411201, People's Republic of China

Supporting Information

ABSTRACT: We reported the favorable cathode buffer layer based on a blend of ZnO nanoparticles (NPs) and TiO_2 nanorods (NRs) applied to inverted solar cells. In addition to the high optical transmittance, the resultant blend film gave a relatively dense film with lower roughness than that of the respective single-component film. This improved the interface contact between the buffer layer and photoactive layer and therefore reduced the contact resistance and leakage current. Moreover, the combination of NRs and NPs increased the efficiency of electron transport and collection by providing both a direct path for electron transport from TiO_2 NRs and a large contact area between ZnO NPs and the active layer. Consequently, both the short-circuit current density (J_{sc}) and fill factor (FF) in the device were improved, leading to an improvement of the device performance. The best power conversion efficiency (PCE) based on the blend film as the buffer layer reached 8.82%, which was preferable to those of a single ZnO NP film (7.76%) and a TiO_2 NR-based device (7.66%).

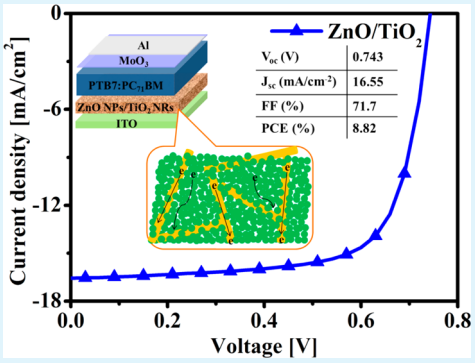

KEYWORDS: *ZnO nanoparticles, TiO_2 nanorods, blend film, cathode buffer layer, inverted solar cells*

1. INTRODUCTION

In the last decades, polymer solar cells (PSCs) have been a hot research topic because of their promising advantages such as low cost, flexibility, and light weight compared with conventional silicon-based solar cells.[1−3] The first bulk-heterojunction PSCs were successfully realized in 1995 by the Heeger group and gave a power conversion efficiency (PCE) of 2.9%.[4] With the development of new donor and acceptor materials and advanced processing techniques flocking in, PSCs with PCEs of 7−9% based on poly(3,4-ethylenedioxythiophene):poly(styrenesulfonate) (PEDOT:PSS) as the hole-transport layer have been documented.[5−8] In the meantime, the erosion of indium−tin oxide (ITO) by acidic PEDOT:PSS and oxidation of an air-sensitive, low-work-function metal cathode become the main factors to influence the long lifetime stability in photovoltaic devices.[9−11] Hence, in addition to increasing PCE, further efforts should be made to improve the device stability.

To solve this issue, one strategy is to use an inverted device architecture. Since the first example reported in 2006,[12,13] the inverted device structure has been extensively studied. So far, PCEs as high as 9.2% have been achieved.[14−16] In an inverted structure, the top electrode, composed of a high-work-function transition-metal oxide (NiO, MoO_3, V_2O_5, and WO_3) layer and a high-work-function metal electrode (Au and Ag), is used to collect the holes.[17−19] Meanwhile, the ITO electrode is modified with a thin film of n-type material such as cesium carbonate (Cs_2CO_3),[20] zinc oxide (ZnO),[13,21] and titanium oxide (TiO_2 and TiO_x)[22,23] as hole-blocking and electron-transport layers (ETLs), which could functionalize the work-function of the ITO electrode. In this way, PEDOT:PSS is replaceable, and new interfacial materials can improve the device stability.

The cathode buffer layer on the ITO electrode is one of the key components of the inverted architecture. Several criteria should be met to obtain a favorable cathode buffer layer for an efficient photovoltaic device, such as good transparency, high electron mobility, favorable morphology, and high electron affinity to collect the electrons. Among n-type metal oxides, ZnO and TiO_2 nanoparticles (NPs) have drawn more attention because of their good transparency, environmental stability, simplicity of process, and low crystallization temperature.[21,24] However, the ZnO NP film presents apparent surface defects due to aggregations, leading to poor electronic coupling and severe back charge recombination.[25,26] Meanwhile, TiO_2 NPs possess wide band gap (3.2 eV) and low electron mobility (10^{-5} cm^2 V^{-1} S^{-1}).[27] One-dimensional TiO_2 nanorods (NRs)

Received: December 6, 2013
Accepted: March 7, 2014
Published: March 7, 2014

support a direct pathway to facilitate electron transport, which has been used in hybrid solar cell investigation.[28−30] However, its relatively low surface-to-volume ratio decreases the contact area and influences electron collection in the photovoltaic device.[31,32] Different methods have been used to address these issues such as doping with metals,[22,33] use of composite materials,[34] incorporation of fullerene derivatives,[25,35−39] and use of hybrids with conjugated molecules.[26,40−43] Those help to improve the contact quality and modify the work function of metal oxides, further increasing the performance of organic solar cells. In comparison, few studies have worked on the combination of metal oxide nanomaterials with various shapes and sizes as a buffer layer in solar cells.[44−46]

In this study, the blend films of ZnO NPs and TiO_2 NRs were embedded in a cathode buffer layer of inverted PSCs. The photoactive materials involved were poly[[4,8-bis[(2-ethylhexyl)oxy]benzo[1,2-*b*:4,5-*b*′]dithiophene-2,6-diyl][3-fluoro-2-[(2-ethylhexyl)carbonyl]thieno[3,4-*b*]thiophenediyl]] (PTB7) as the electron donor and [6,6]phenyl-C71-butyric acid methyl ester ($PC_{71}BM$) as the electron acceptor. We successfully demonstrated highly efficient PSCs with an average PCE of 8.58% under simulated solar illumination (AM 1.5G 100 mW cm^{-2}), which was increased by 15.6% and 12.6% in comparison with those of devices based solely on the ZnO NP film (7.42%) and TiO_2 NR film (7.62%), respectively. To understand the efficiency enhancement, the optical property, surface morphology, composition structure, energy-level property, and electrical properties of the blend film were investigated by multiple measurements such as UV−vis absorption, scanning electron microscopy (SEM), atomic force microscopy (AFM), X-ray photoelectron spectroscopy (XPS), and ultraviolet photoelectron spectroscopy (UPS). The results showed that the interfacial blend film possesses favorable optoelectronic properties and superior film morphology, which improve interfacial contact to facilitate charge collection.

2. EXPERIMENTAL SECTION

Reagent and Materials. Indium−tin oxide (ITO)-coated glass substrates were purchased from CSG Holding Co., Ltd. (China; $R_s \leq 10\ \Omega/\square$; $T_r \geq 83\%$). Electron-donor material PTB7 was purchased from 1-material Chemscitech, and electron-acceptor $PC_{71}BM$ was purchased from Nano-C. MoO_3 was obtained from Alfa Aesar. Chlorobenzene was provided by Sigma-Aldrich. In addition, zinc acetate dihydrate [$Zn(Ac)_2{\cdot}2H_2O$], potassium hydroxide (KOH), methanol, and chloroform were purchased from Sinopharm Chemical Reagent Co. and used as received.

Preparation of ZnO NPs. ZnO NPs were prepared according to the procedures.[47,48] We used chloroform (5 mL) to dissolve the NPs to obtain a solution with a concentration of 70 mg mL^{-1} on average. Then the concentration of 15 mg mL^{-1} ZnO was obtained by dilution of the original solution with chloroform and a small amount methanol (10 vol %).

Preparation of TiO_2 NRs. TiO_2 NRs were fabricated following the process reported by Weller et al.[49] The as-synthesized TiO_2 NRs were usually capped with a long-chain ligand of oleic acid (OA), which suppressed charge transfer. Hence, OA of TiO_2 NRs was removed by ligand exchange with pyridine, according to the literature.[50] Finally, TiO_2 NRs were dissolved in chloroform with a concentration of 20 mg mL^{-1}.

Preparation of Cathode Buffer Layers. The blend solutions of ZnO NPs and TiO_2 NRs with different weight ratios were prepared by mixing the respective solutions of ZnO NPs (15 mg mL^{-1}) and TiO_2 NRs (20 mg mL^{-1}), and the total concentration was 15 mg mL^{-1}.

Device Fabrication and Characterization. The devices were fabricated on ITO-coated glass substrates cleaned with a sequence of detergent, deionized water, acetone, and isopropyl alcohol for 15 min in an ultrasonic bath, dried with a nitrogen stream, and subsequently treated with UV−ozone for 30 min. The ZnO NP solution, TiO_2 NR solution, and mixed solution were spin-coated onto the ITO substrates, respectively. Then the ZnO NP and TiO_2 NR films were annealed at 80 and 150 °C for 10 min, respectively. The blend film was treated at different annealing temperatures (80, 120, 150, and 200 °C) for 10 min to figure out the optimal conditions. The favorable thickness for the blend film was tested as 45 nm. The blend solution of PTB7:$PC_{71}BM$ (10:15 weight ratio) in chlorobenzene was then spin-coated at 1500 rpm for 120 s on top of the buffer layers. Finally, device fabrication was finished by thermal evaporation of 10 nm of MoO_3 and 100 nm of Al under a vacuum of about 1×10^{-6} mbar, and the device area was 0.04 cm^2. *J*−*V* characterization was done using a Keithley 2400 source measure unit under AM 1.5G simulated solar illumination.

Cathode Buffer Layer Characterization. Optical transmittance spectra were recorded using a UV-3300 spectrophotometer. The surface morphology and film roughness of the specimens were tested by SEM and AFM. SEM (S-4800) measurements were done at an acceleration voltage of 8 kV. AFM measurements were done in tapping mode using a Veeco dimension V atomic force microscope. XPS and UPS spectra were taken with a Kratos AXIS ULTRA^{DLD} UPS/XPS system (Kratos Analytical, Manchester, U.K.).

3. RESULTS AND DISCUSSION

Figure 1 shows the structures of PTB7 and $PC_{71}BM$, as well as an inverted device structure. The interfacial blend film was

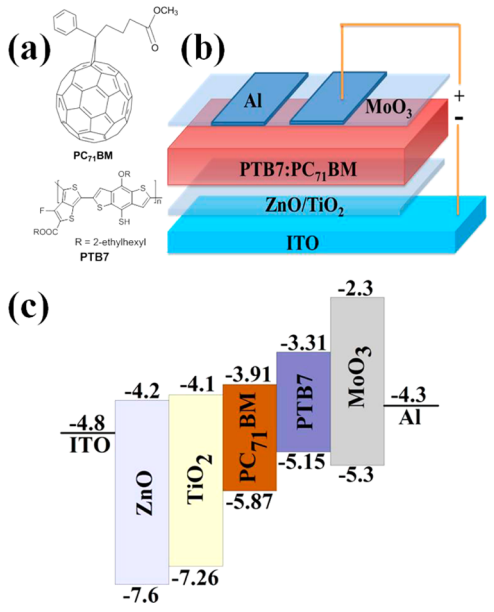

Figure 1. (a) Structures of PTB7 and $PC_{71}BM$. (b) Device structure of inverted PSCs with blend films of ZnO NPs and TiO_2 NRs as the cathode buffer layer. (c) Corresponding energy-level diagram of each component of the device.

obtained by spin-coating the mixed solution of ZnO NPs and TiO_2 NRs onto the ITO electrode. The energy-level diagram of the materials involved in the device is depicted in Figure 1c. The lowest unoccupied molecular orbital (LUMO) and highest occupied molecular orbital (HOMO) energy levels of PTB7 and $PC_{71}BM$ were taken from the literature.[16,51] The energy levels of ZnO NPs and TiO_2 NRs were measured by UPS and UV absorption edge. It is obvious that the conduction band

dx.doi.org/10.1021/am405622q | ACS Appl. Mater. Interfaces 2014, 6, 4074−4080

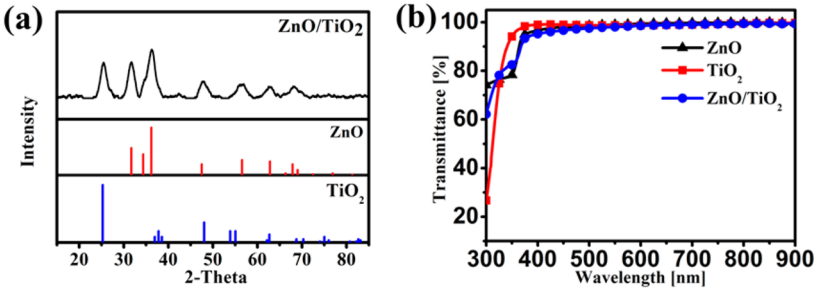

Figure 2. (a) XRD pattern for the ZnO/TiO_2 blend film after annealing at 120 °C for 10 min. (b) UV−vis transmittance spectra of the ZnO NP, TiO_2 NR, and ZnO/TiO_2 blend films on quartz substrates.

(CB) of TiO_2 is very close to the LUMO of $PC_{71}BM$ and the CB of ZnO, which indicates that electrons can be easily transferred to the ITO electrode through the blend buffer layer. Moreover, the valence bands of ZnO (−7.6 eV) and TiO_2 (−7.26 eV) are lower than the HOMO levels of PTB7 (−5.15 eV) and $PC_{71}BM$ (−5.87 eV), which block hole transport from PTB7 to the ITO electrode. Thus, from the viewpoint of energy levels, photogenerated carriers can efficiently transport electrodes without significant interfacial energy loss.

The crystallinity of the blend film was investigated by X-ray diffraction (XRD), and the results are shown in Figure 2a. The typical XRD patterns of the blend film confirmed the existence of wurtzite-type ZnO and anatase-type TiO_2 crystalline phases, which is in good agreement with the previously reported results.[48,49] No other crystalline phase was found in the XRD pattern, indicating that the matrix is a physical mixture of ZnO NPs and TiO_2 NRs. In addition, XPS data are presented in Figure S1 in the Supporting Information (SI). The spectra further gave proof of the existence of ZnO NPs and TiO_2 NRs in the blend film. In inverted solar cells, high transparency was required for the cathode buffer layer. Figure 2b compares the UV−vis transmittance spectra (300−900 nm) of the ZnO NP, TiO_2 NR, and ZnO/TiO_2 blend films on quartz substrates. It is apparent that the three films have high optical transmittance, which is suitable for the buffer layer in organic solar cell. The transmittance near 100% in the wavelength region of 400−900 nm means that light absorption for the photoactive layer can be retained. In the short-wavelength region, the blend film showed partial absorption because of the wide band gap. The operational stability of PSCs could be improved by absorbing ultraviolet light, which usually gives rise to photodegradation of organic materials.[52]

In addition to transmittance, the morphology of the buffer layer is very crucial for the interfacial electrical property.[53,54] The surface morphologies of the films were investigated by tapping-mode AFM and SEM. Parts a−c of Figure 3 present the AFM images of the ZnO NP, TiO_2 NR, and blend films, respectively. The root-mean-square roughness of the three films was calculated as 12.6, 6.58, and 5.42 nm, respectively. The blend film showed the smoothest surface among the three films. This means that the blend film obtained good contact quality with the PTB7:$PC_{71}BM$ active layer and decreased the contact resistance so as to improve charge collection more effectively.[55]

SEM images were employed to further investigate the surface morphology of the three films. In Figure 3d, the ZnO NP film is composed of NPs that possess a high surface-to-volume ratio and increased contact area with the photoactive layer so as to improve the electron collection efficiency. However, ZnO NPs easily form aggregations. Many voids are found on the surface

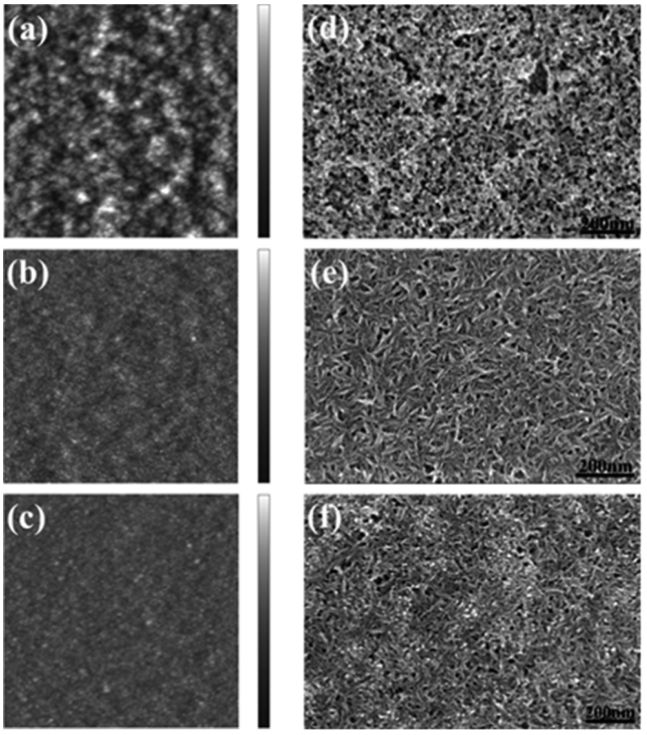

Figure 3. AFM images of the surface morphology of (a) the ZnO NP film, (b) the TiO_2 NR film, and (c) the blend film of ZnO/TiO_2 (with a scan size of 5 μm × 5 μm and a height bar of 200 nm). SEM images of the morphology of (d) the ZnO NP film, (e) the TiO_2 NR film and (f) the blend film of ZnO/TiO_2 (scale bar: 200 nm).

in the images. The aggregations are thought to be the origin of high roughness. Figure 3e shows the surface morphology of the TiO_2 NR film, and some voids exist on the surface similar to the ZnO NP film. The blend film composed of ZnO NPs and TiO_2 NRs gives the best surface morphology among the three films. It presents relatively compact film morphology and gives the fewest surface voids. According to the literature, the leakage current is caused by voids of the buffer layer in the devices.[26] So, the blend film shows favorable interface properties for photovoltaic applications.

The current density−voltage (J−V) characteristics under AM 1.5G irradiation (100 mW cm^{-2}) of inverted PTB7:$PC_{71}BM$ solar cells with different electron-transport layers were investigated and are shown in Figure 4. The extracted device parameters, as well as the series resistance (R_s) and shunt resistance (R_{sh}) of all of the devices, are summarized in Table 1. The device based on a ZnO NP cathode buffer layer gave a typical open-circuit voltage (V_{oc}) of 0.732 V, J_{sc} of 15.27 mA

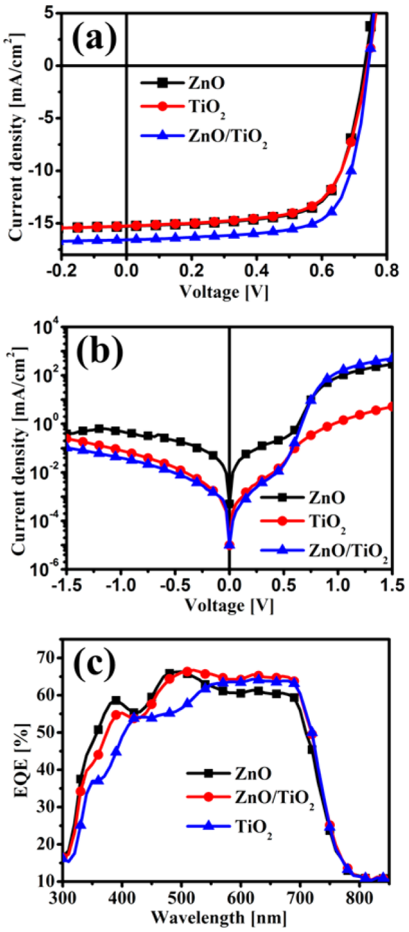

Figure 4. (a) Illuminated and (b) dark J–V characteristics of ITO/interlayer/PTB7:$PC_{71}BM$/MoO_3/Al architecture with different cathode buffer layers. (c) EQE data of devices based on PTB7:$PC_{71}BM$ blends using the ZnO NP, TiO_2 NR, and ZnO/TiO_2 blend films as cathode buffer layers measured in air with a larger spot size than the device area.

Table 1. Summary of the Photovoltaic Parameters of PTB7:$PC_{71}BM$ Devices Fabricated with Different Cathode Buffer Layers

interlayer	V_{oc} [V]	J_{sc} [mA cm^{-2}]	FF [%]	R_s [Ω cm^2]	R_{sh} [kΩ cm^2]	best/average PCE [%][a]
ZnO	0.732	15.27	69.4	4.92	1.01	7.76/7.42
TiO_2	0.740	15.23	68.0	5.92	0.86	7.66/7.62
ZnO/TiO_2	0.743	16.55	71.7	4.20	1.11	8.82/8.58

[a]The parameters of PCEs were averaged over six devices. The device parameter distribution map was presented in Figure S5 in the SI

cm^{-2}, and FF of 69.4%, corresponding to a PCE of 7.76%. Meanwhile, the device based on the TiO_2 NR cathode buffer layer showed V_{oc} of 0.740 V, J_{sc} of 15.23 mA cm^{-2}, FF of 68.0%, and PCE of 7.66%. When the optimal weight ratio (10:5 mg mL^{-1}) was used in the blend buffer layer, the device presented V_{oc} of 0.743 V, J_{sc} of 16.55 mA cm^{-2}, and FF of 71.7%, giving PCEs as high as 8.82%. Figure 4c shows the external quantum efficiency (EQE) data of the optimal device based on the blend film. J_{EQE} calculated from integration of the EQE spectrum from 300 to 800 nm is consistent with J_{sc} obtained from the J–V results shown above. These results demonstrated the superior interface properties of the blend film. Table 1 presents all of the device parameters with similar V_{oc} values. However, J_{sc} and FF of devices based on the blend film were improved dramatically relative to the devices using ZnO NPs and TiO_2 NRs as buffer layers, which represent improvements of 13.5% and 15.0% in the performance, respectively. From the dark J–V characteristics in Figure 4b, the device based on the blend film exhibited excellent diode characteristics with a lower leakage current and a higher rectification ratio. In contrast, the device based on the ZnO NP buffer layer presents a higher leakage current, resulting from the voids in the surface.[56] To investigate the origin of performance enhancement, R_s and R_{sh} were also measured. R_s (4.20 Ω cm^2) of devices based on the blend film was lower than those of the ZnO NP film (4.92 Ω cm^2) and TiO_2 NR film (5.92 Ω cm^2). Moreover, R_{sh} (1.11 kΩ cm^2) of devices based on the blend film was higher than those of the ZnO NP film (1.01 kΩ cm^2) and TiO_2 NR film (0.86 kΩ cm^2). According to the literature,[26,54] the decreased R_s and increased R_{sh} contributed to the device performance by improving FF and J_{sc}.

To further probe the thermal treatment effect of the blend buffer layer on the device performance of the inverted PSCs, the photovoltaic devices were studied by changing the temperature from 80 to 200 °C for 10 min, and the results are shown in Figure S8 in the SI and summarized in Table 2.

Table 2. Detailed Parameters of the Device Performance Using Blend Films with Different Annealing Temperatures

temperature [°C]	V_{oc} [V]	J_{sc} [mA cm^{-2}]	FF [%]	R_s [Ω cm^2]	R_{sh} [kΩ cm^2]	best/average PCE [%]
80	0.720	14.98	68.4	5.96	0.90	7.38/7.25
120	0.743	16.55	71.7	4.20	1.11	8.82/8.58
150	0.743	16.17	71.2	4.36	1.23	8.55/8.43
200	0.734	16.24	69.0	4.28	0.94	8.23/8.04

With an increase of the annealing temperature from 80 to 120 °C, V_{oc}, J_{sc}, and FF of the devices increased and thus PCE increased from 7.38% to 8.81%. This result was attributed to the remaining pyridine in the blend film, which obstructs electron collection and electron transport.[44,57] Pyridine was removed after annealing at 120 °C, resulting in an improvement of the device performance. However, when the annealing temperature was further increased to 150 and 200 °C, the device performance was gradually decreased. The possible reason was that the contact quality of the buffer layer with the electrode became poor, leading to slightly higher contact resistance. To summarize, the appropriate thermal treatment condition was 120 °C for 10 min.

Figure 5 illustrates the mechanism of electron (e^-) transport in the blend film. Electrons were transferred from the ZnO NP film to the surface of the collector electrode (e.g., ITO substrate) through a zigzag pathway, in which the electrons leap from one NP to the adjacent NP according to the literature.[46,58] The increase of the electron-transport pathway results in increments of bulk resistance and chances of electron–hole recombination, resulting from the surface defect from ZnO NP aggregations.[26] In the meantime, TiO_2 NRs provide a direct pathway for electron transport, avoiding long-range travel among ZnO NPs, which supports an effective means for electron transport.[31,32] However, PCE of devices based on the TiO_2 NR film is lower than that of the ZnO NP film, mainly because of insufficient contact area with the active layer. The blend film in nanoscale provides both a large surface area to

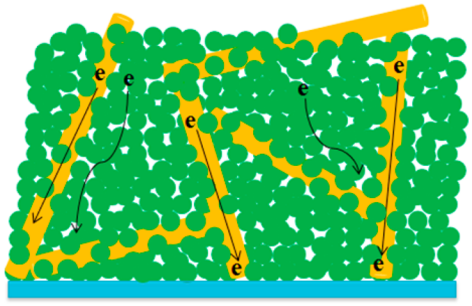

Figure 5. Schematic illustration of electron (e^-) transport of the blend film of ZnO NPs and TiO_2 NRs as the cathode buffer layer.

promote charge collection and a direct pathway for high-efficient electron transfer, resulting in the improvement of J_{sc} and FF in the devices. The combination of ZnO NPs and TiO_2 NRs can make use of both features working as the cathode buffer layer and facilitate electron transport from the active layer to the ITO electrode.

4. CONCLUSION

In conclusion, we have developed a new cathode buffer layer based on a combination of ZnO NPs and TiO_2 NRs to take advantage of their respective features. The optimized blend film gave a dense film with low roughness. It can facilitate electron collection and improve the electron-transport efficiency. Also, high-efficiency inverted PSC was demonstrated based on PTB7:PC_{71}BM, giving an average PCE of 8.58%, which increases by 15.6% and 12.6% in comparison with solely the ZnO NP film (7.42%) and solely the TiO_2 NR film (7.62%), respectively. The results not only indicated that the blend film was the superior cathode buffer layer but also provided the method that a combination of inorganic nanomaterials with particular morphology gave multiple advantages in the fabrication of high-performance PSCs.

■ ASSOCIATED CONTENT

Supporting Information

Cross-sectional SEM image and XPS spectra of the blend film, UV−vis absorption spectra of ZnO NP and TiO_2 NR films, UPS spectrum of the ZnO NP film, device parameter distribution map using ZnO, ZnO/TiO_2, and TiO_2 as the buffer layer in a PTB7:PCB_{71}M system, different blend ratio dependences of ZnO NPs/TiO_2 NRs on the device performance, different thickness dependences of a blend film on the device performance, $J-V$ characteristics, and AFM images of the device performance using a blend film with different annealing temperatures. This material is available free of charge via the Internet at http://pubs.acs.org.

■ AUTHOR INFORMATION

Corresponding Authors

*E-mail: jiutonggang@nimte.ac.cn.
*E-mail: lixiaofang@iccas.ac.cn.
*E-mail: fangjf@nimte.ac.cn.

Notes

The authors declare no competing financial interest.

■ ACKNOWLEDGMENTS

The authors gratefully acknowledge support of the National Natural Science Foundation of China (Grants 51202264 and 51273208) and the Specialized Research Fund for the Spring Buds Talent Program (Grant Y20804RA02). The work was also supported by the Hundred Talent Program of Chinese Academy of Sciences and the Starting Research Fund of Team Talent (Grant Y10801RA01) in NIMTE.

■ REFERENCES

(1) Chen, J.; Cao, Y. Development of Novel Conjugated Donor Polymers for High-Efficiency Bulk-Heterojunction Photovoltaic Devices. *Acc. Chem. Res.* **2009**, *42*, 1709−1718.
(2) Krebs, F. C.; Tromholt, T.; Jørgensen, M. Upscaling of Polymer Solar Cell Fabrication using full Roll-to-roll Processing. *Nanoscale* **2010**, *2*, 873−886.
(3) Cai, W.; Gong, X.; Cao, Y. Polymer Solar Cells: Recent Development and Possible Routes for Improvement in the Performance. *Sol. Energy Mater. Sol. Cells* **2010**, *94*, 114−127.
(4) Yu, G.; Gao, J.; Hunmelen, J. C.; Wudl, F.; Heeger, A. J. Polymer Photovoltaic Cells: Enhanced Efficiencies via a Network of Internal Donor-Acceptor Heterojunctions. *Science* **1995**, *270*, 1789−1791.
(5) Lu, L.; Luo, Z.; Xu, T.; Yu, L. Cooperative Plasmonic Effect of Ag and Au Nanoparticles on Enhancing Performance of Polymer Solar Cells. *Nano Lett.* **2013**, *13*, 59−64.
(6) Liang, Y.; Xu, Z.; Xia, J.; Tsai, S.-T.; Wu, Y.; Li, G.; Ray, C.; Yu, L. For the Bright Future-bulk Heterojunction Polymer Solar Cells with Power Conversion Efficiency of 7.4%. *Adv. Mater.* **2010**, *22*, E135−E138.
(7) Zhang, M.; Gu, Y.; Guo, X.; Liu, F.; Zhang, S.; Huo, L.; Russell, T. P.; Hou, J. Efficient Polymer Solar Cells Based on Benzothiadiazole and Alkylphenyl Substituted Benzodithiophene with a Power Conversion Efficiency over 8%. *Adv. Mater.* **2013**, *25*, 4944−4949.
(8) Huo, L.; Zhang, S.; Guo, X.; Xu, F.; Li, Y.; Hou, J. Replacing Alkoxy Groups with Alkylthienyl Groups: a Feasible Approach to Iimprove the Properties of Photovoltaic Polymers. *Angew. Chem., Int. Ed.* **2011**, *50*, 9697−9702.
(9) Jong, M. P. d.; Ijzendoorn, L. J. v.; Voigt, M. J. A. d. Stability of the Interface between Indium-tin-oxide and poly(3,4-ethylenedioxythiophene)/poly(styrenesulfonate) in Polymer Light-emitting Diodes. *Appl. Phys. Lett.* **2000**, *77*, 2255−2257.
(10) Kawano, K.; Pacios, R.; Poplavskyy, D.; Nelson, J.; Bradley, D. D. C.; Durrant, J. R. Degradation of Organic Solar Cells due to Air Exposure. *Sol. Energy Mater. Sol. Cells* **2006**, *90*, 3520−3530.
(11) Norrman, K.; Gevorgyan, S. A.; Krebs, F. C. Water-Induced Degradation of Polymer Solar Cells Studied by $H_2{}^{18}O$ Labeling. *ACS Appl. Mater. Interfaces* **2009**, *1*, 102−112.
(12) Li, G.; Chu, C.-W.; Shrotriya, V.; Huang, J.; Yang, Y. Efficient Inverted Polymer Solar Cells. *Appl. Phys. Lett.* **2006**, *88*, 253503.
(13) White, M. S.; Olson, D. C.; Shaheen, S. E.; Kopidakis, N.; Ginley, D. S. Inverted Bulk-heterojunction Organic Photovoltaic Device using a Solution-derived ZnO Underlayer. *Appl. Phys. Lett.* **2006**, *89*, 143517.
(14) Chen, L.-M.; Hong, Z.; Li, G.; Yang, Y. Recent Progress in Polymer Solar Cells: Manipulation of Polymer:Fullerene Morphology and the Formation of Efficient Inverted Polymer Solar Cells. *Adv. Mater.* **2009**, *21*, 1434−1449.
(15) Xu, Z.; Chen, L.-M.; Yang, G.; Huang, C.-H.; Hou, J.; Wu, Y.; Li, G.; Hsu, C.-S.; Yang, Y. Vertical Phase Separation in Poly(3-hexylthiophene): Fullerene Derivative Blends and its Advantage for Inverted Structure Solar Cells. *Adv. Funct. Mater.* **2009**, *19*, 1227−1234.
(16) He, Z.; Zhong, C.; Su, S.; Xu, M.; Wu, H.; Cao, Y. Enhanced Power-conversion Efficiency in Polymer Solar Cells using an Inverted Device Structure. *Nat. Photonics* **2012**, *190*, 591−595.
(17) Irwin, M. D.; Buchholz, D. B.; Hains, A. W.; Chang, R. P. H.; Marks, T. J. p -Type Semiconducting Nickel Oxide as an Efficiency-enhancing Anode Interfacial Layer in Polymer Bulk-heterojunction Solar Cells. *Proc. Natl. Acad. Sci. U. S. A.* **2008**, *105*, 2783−2787.

(18) Murase, S.; Yang, Y. Solution Processed MoO_3 Interfacial Layer for Organic Photovoltaics Prepared by a Facile Synthesis Method. *Adv. Mater.* **2012**, *24*, 2459−2462.
(19) Han, S.; Shin, W. S.; Seo, M.; Gupta, D.; Moon, S.-J.; Yoo, S. Improving Performance of Organic Solar Cells Using Amorphous Ttungsten Oxides as an Iinterfacial Buffer Layer on Transparent Anodes. *Org. Electron.* **2009**, *10*, 791−797.
(20) Liao, H.-H.; Chen, L.-M.; Xu, Z.; Li, G.; Yang, Y. Highly Efficient Inverted Polymer Solar Cell by Low Temperature Annealing of Cs_2CO_3 Interlayer. *Appl. Phys. Lett.* **2008**, *92*, 173303.
(21) Sun, Y.; Seo, J. H.; Takacs, C. J.; Seifter, J.; Heeger, A. J. Inverted Polymer Solar Cells Integrated with a Low-Temperature-Annealed Sol−Gel-Derived ZnO Film as an Electron Transport Layer. *Adv. Mater.* **2011**, *23*, 1679−1683.
(22) Waldauf, C.; Morana, M.; Denk, P.; Schilinsky, P.; Coakley, K.; Choulis, S. A.; Brabec, C. J. Highly Efficient Inverted Organic Photovoltaics Using Solution Based Titanium Oxide as Electron Selective Contact. *Appl. Phys. Lett.* **2006**, *89*, 233517.
(23) Zhang, D.; Choy, W. C. H.; Xie, F.; Sha, W. E. I.; Li, X.; Ding, B.; Zhang, K.; Huang, F.; Cao, Y. Plasmonic Electrically Functionalized TiO_2 for High-Performance Organic Solar Cells. *Adv. Funct. Mater.* **2013**, *23*, 4255−4261.
(24) Salim, T.; Yin, Z.; Sun, S.; Huang, X.; Zhang, H.; Lam, Y. M. Solution-Processed Nanocrystalline TiO_2 Buffer Layer Used for Improving the Performance of Organic Photovoltaics. *ACS Appl. Mater. Interfaces* **2011**, *3*, 1063−1067.
(25) Hau, S. K.; Yip, H.-L.; Ma, H.; Jen, A. K.-Y. High Performance Ambient Processed Inverted Polymer Solar Cells Through Interfacial Modification with a Fullerene Self-assembled Monolayer. *Appl. Phys. Lett.* **2008**, *93*, 233304.
(26) Shao, S.; Zheng, K.; Pullerits, T.; Zhang, F. Enhanced Performance of Inverted Polymer Solar Cells by Using Poly(ethylene oxide)-Modified ZnO as an Electron Transport Layer. *ACS Appl. Mater. Interfaces* **2013**, *5*, 380−385.
(27) Park, K.; Zhang, Q.; Garcia, B. B.; Zhou, X.; Jeong, Y.-H.; Cao, G. Effect of an Ultrathin TiO_2 Layer Coated on Submicrometer-Sized ZnO Nanocrystallite Aggregates by Atomic Layer Deposition on the Performance of Dye-Sensitized Solar Cells. *Adv. Mater.* **2010**, *22*, 2329−2332.
(28) Lin, Y.-T.; Zeng, T.-W.; Lai, W.-Z.; Chen, C.-W.; Lin, Y.-Y.; Chang, Y.-S.; Su, W.-F. Efficient Photoinduced Charge Transfer in TiO_2 Nanorod/conjugated Polymer Hybrid Materials. *Nanotechnology* **2006**, *17*, 5781−5785.
(29) Chuang, C.-H.; Lin, Y.-Y.; Tseng, Y.-H.; Chu, T.-H.; Lin, C.-C.; Su, W.-F.; Chen, C.-W. Nanoscale Morphology Control of Polymer/TiO_2 Nanocrystal Hybrids: Photophysics, Charge Generation, Charge Transport, and Photovoltaic Properties. *J. Phys. Chem. C* **2010**, *114*, 18717−18724.
(30) Li, S.-S.; Chang, C.-P.; Lin, C.-C.; Lin, Y.-Y.; Chang, C.-H.; Yang, J.-R.; Chu, M.-W.; Chen, C.-W. Interplay of Three-Dimensional Morphologies and Photocarrier Dynamics of Polymer/TiO_2 Bulk Heterojunction Solar Cells. *J. Am. Chem. Soc.* **2011**, *133*, 11614−11620.
(31) Yu, K.; Chen, J. Enhancing Solar Cell Efficiencies through 1-D Nanostructures. *Nanoscale Res. Lett.* **2009**, *4*, 1−10.
(32) Adachi, M.; Murata, Y.; Takao, J.; Jiu, J.; Sakamoto, M.; Wang, F. Highly Efficient Dye-Sensitized Solar Cells with a Titania Thin-Film Electrode Composed of a Network Structure of Single-Crystal-like TiO_2 Nanowires Made by the "Oriented Attachment" Mechanism. *J. Am. Chem. Soc.* **2004**, *126*, 14943−14949.
(33) Gadisa, A.; Liu, Y.; Samulski, E. T.; Lopez, R. Role of Thin n-Type Metal-Oxide Interlayers in Inverted Organic Solar Cells. *ACS Appl. Mater. Interfaces* **2012**, *4*, 3846−3851.
(34) Liu, J.; Shao, S.; Fang, G.; Meng, B.; Xie, Z.; Wang, L. High-Efficiency Inverted Polymer Solar Cells with Transparent and Work-Function Tunable MoO_3−Al Composite Film as Cathode Buffer Layer. *Adv. Mater.* **2012**, *24*, 2774−2779.
(35) Cheng, Y.-J.; Hsieh, C.-H.; He, Y.; Hsu, C.-S.; Li, Y. Combination of Indene-C60 Bis-Adduct and Cross-Linked Fullerene Interlayer Leading to Highly Efficient Inverted Polymer Solar Cells. *J. Am. Chem. Soc.* **2010**, *132*, 17381−17383.
(36) Cheng, Y.-J.; Cao, F.-Y.; Lin, W.-C.; Chen, C.-H.; Hsieh, C.-H. Self-Assembled and Cross-Linked Fullerene Interlayer on Titanium Oxide for Highly Efficient Inverted Polymer Solar Cells. *Chem. Mater.* **2011**, *23*, 1512−1518.
(37) Chang, Y. M.; Leu, C. Y. Conjugated Polyelectrolyte and Zinc Oxide Stacked Structure as an Interlayer in Highly Efficient and Stable Organic Photovoltaic Cells. *J. Mater. Chem. A* **2013**, *1*, 6446−6451.
(38) Kyaw, A. K. K.; Wang, D. H.; Gupta, V.; Zhang, J.; Chand, S.; Bazan, G. C.; Heeger, A. J. Efficient Solution-Processed Small-Molecule Solar Cells with Inverted Structure. *Adv. Mater.* **2013**, *25*, 2397−2402.
(39) Savva, A.; Petraki, F.; Elefteriou, P.; Sygellou, L.; Voigt, M.; Giannouli, M.; Kennou, S.; Nelson, J.; Bradley, D. D. C.; Brabec, C. J.; Choulis, S. A. The Effect of Organic and Metal Oxide Interfacial layers on the Performance of Inverted Organic Photovoltaics. *Adv. Energy Mater.* **2013**, *3*, 391−398.
(40) Small, C. E.; Chen, S.; Subbiah, J.; Amb, C. M.; Tsang, S.-W.; Lai, T.-H.; Reynolds, J. R.; So, F. High-efficiency Inverted Dithienogermole−thienopyrro-lodione-based Polymer Solar Cells. *Nat. Photonics* **2012**, *6*, 115−120.
(41) Hu, T.; Li, F.; Yuan, K.; Chen, Y. Efficiency and Air-Stability Improvement of Flexible Inverted Polymer Solar Cells Using ZnO/Poly(ethylene glycol) Hybrids as Cathode Buffer Layers. *ACS Appl. Mater. Interfaces* **2013**, *5*, 5763−5770.
(42) Liu, H.; Xu, J.; Li, Y.; Li, Y. Aggregate Nanostructures of Organic Molecular Materials. *Acc. Chem. Res.* **2010**, *43*, 1496−1508.
(43) Liu, H.; Zuo, Z.; Guo, Y.; Li, Y.; Li, Y. Supramolecular Interactions at the Inorganic−Organic Interface in Hybrid Nanomaterials. *Angew. Chem., Int. Ed.* **2010**, *49*, 2705−2707.
(44) Lin, Y.-H.; Yang, P.-C.; Huang, J.-S.; Huang, G.-D.; Wang, I.-J.; Wu, W.-H.; Lin, M.-Y.; Su, W.-F.; Lin, C.-F. High-efficiency Inverted Polymer Solar Cells with Solution-processed Metal Oxides. *Sol. Energy Mater. Sol. Cells* **2011**, *95*, 2511−2515.
(45) Liu, J.; Shao, S.; Meng, B.; Fang, G.; Xie, Z.; Wang, L.; Li, X. Enhancement of Inverted Polymer Solar Cells with Solution-processed ZnO−TiO_X Composite as Cathode Buffer Layer. *Appl. Phys. Lett.* **2012**, *100*, 213906.
(46) Bai, Y.; Yu, H.; Li, Z.; Amal, R.; Lu, G. Q. M.; Wang, L. In Situ Growth of a ZnO Nanowire Network within a TiO_2 Nanoparticle Film for Enhanced Dye-Sensitized Solar Cell Performance. *Adv. Mater.* **2012**, *24*, 5850−5856.
(47) Pacholski, C.; Kornowski, A.; Weller, H. Self-Assembly of ZnO: From Nanodots to Nanorods. *Angew. Chem., Int. Ed.* **2002**, *41*, 1188−1191.
(48) Beek, W. J. E.; Wienk, M. M.; Kemerink, M.; Yang, X.; Janssen, R. A. J. Hybrid Zinc Oxide Conjugated Polymer Bulk Heterojunction Solar Cells. *J. Phys. Chem. B* **2005**, *109*, 9505−9516.
(49) Cozzoli, P. D.; Kornowski, A.; Weller, H. Low-Temperature Synthesis of Soluble and Processable Organic-Capped Anatase TiO_2 Nanorods. *J. Am. Chem. Soc.* **2003**, *125*, 14539−14548.
(50) Lin, Y.-Y.; Chu, T.-H.; Li, S.-S.; Chuang, C.-H.; Chang, C.-H.; Su, W.-F.; Chang, C.-P.; Chu, M.-W.; Chen, C.-W. Interfacial Nanostructuring on the Performance of Polymer/TiO_2 Nanorod Bulk Heterojunction Solar Cells. *J. Am. Chem. Soc.* **2009**, *131*, 3644−3649.
(51) Tan, Z. a.; Zhang, W.; Qian, Z. Z. D.; Huang, Y.; Hou, J.; Li, Y. High-Performance Inverted Polymer Solar Cells with Solution-Processed Titanium Chelate as Electron-Collecting Layer on ITO Electrode. *Adv. Mater.* **2012**, *24*, 1476−1481.
(52) Yang, T.; Cai, W.; Qin, D.; Wang, E.; Lan, L.; Gong, X.; Peng, J.; Cao, Y. Solution-Processed Zinc Oxide Thin Film as a Buffer Layer for Polymer Solar Cells with an Inverted Device Structure. *J. Phys. Chem. C* **2010**, *114*, 6849−6853.
(53) Shrotriya, V.; Li, G.; Yao, Y.; Chu, C.-W.; Yang, Y. Transition Metal Oxides as the Buffer Layer for Polymer Photovoltaic Cells. *Appl. Phys. Lett.* **2006**, *88*, 073508.

(54) Liang, Z.; Zhang, Q.; Wiranwetchayan, O.; Xi, J.; Yang, Z.; Park, K.; Li, C.; Cao, G. Effects of the Morphology of a ZnO Buffer Layer on the Photovoltaic Performance of Inverted Polymer Solar Cells. *Adv. Funct. Mater.* **2012**, *22*, 2194−2201.
(55) Thompson, B. C.; Frechet, J. M. J. Polymer−Fullerene Composite Solar Cells. *Angew. Chem., Int. Ed.* **2008**, *47*, 58−77.
(56) Chou, C.-H.; Kwan, W. L.; Hong, Z.; Chen, L.-M.; Yang, Y. A Metal−Oxide Interconnection Layer for Polymer Tandem Solar Cells with an Inverted Architecture. *Adv. Mater.* **2011**, *23*, 1282−1286.
(57) Zeng, T.-W.; Lo, H.-H.; Chang, C.-H.; Lin, Y.-Y.; Chen, C.-W.; Su, W.-F. Hybrid Poly(3-hexylthiophene)/titanium Dioxide Nanorods Material for Solar Cell Applications. *Sol. Energy Mater. Sol. Cells* **2009**, *93*, 952−957.
(58) Wong, D. K.-P.; Ku, C.-H.; Chen, Y.-R.; Chen, G.-R.; Wu, J.-J. Enhancing Electron Collection Efficiency and Effective Diffusion Length in Dye-Sensitized Solar Cells. *ChemPhysChem* **2009**, *10*, 2698−2702.